Proceedings of the Korean Nuclear Society Spring Meeting
Kwangju, Korea, May 2002

Simulation of Core Melt Progression Using a Simulant Metal Alloy

Seung Dong Lee, Kune Yull Suh*, Goon Cherl Park, Un Chul Lee

Seoul National University
San 56-1 Sillim-Dong, Kwanak-Gu, Seoul, 151-742, Korea
*Phone: +82-2-8808324, Fax: +82-2-889-2688, Email: kysuh@snu.ac.kr

Abstract

Numerous experiments were conducted to address when and how the core can lose its original geometry, what geometries are formed, and in what processes the core materials are transported to the lower plenum of the reactor pressure vessel during a severe accident. Core degradation progresses along the line of clad ballooning, clad oxidation, material interaction, metallic blockage, molten pool formation, melt progression, and relocation to the lower head. Relocation into the lower plenum may occur from the lateral periphery or from the bottom of the core depending upon the thermal and physical states of the pool. Determining the quantities and rate of molten material transfer to the lower head is important since significant amounts of molten material relocated to the lower head can threaten the vessel integrity by steam explosion and thermal and mechanical attack of the melt. In this paper the focus is placed on the melt flow regime on a cylindrical fuel rod utilizing the LAMDA (Lumped Analysis of Melting in Degrading Assemblies) facility at the Seoul National University. The downward relocation of the molten material is a combination of the external film flow and the internal pipe flow. The heater rods are 0.8 m long and are coated by a low-temperature melting metal alloy. The electrical internal heating method is employed during the test. External heating is adopted to simulate the exothermic Zircaloy-steam reaction. Tests are conducted in several quasi-steady-state conditions. Given the variable boundary conditions including the heat flux and the water level, observation is made for the melting location, progression, and the mass of molten material. Finally, the core melt progression model is developed from the visual inspection and quantitative analysis of the experimental data. As the core material relocates downwards a blockage may be formed and grow both radially and axially. The velocity of the melt can be calculated from a force balance between the gravity and frictional losses at the melt-rod interface. When the heater rod is uncovered completely, the melt progression is initiated at the mid-point, which is the hot spot in the rod. However, the melting location is elevated as the water level rises because of the downward heat transfer. Considering the melt flow as a film, the steady-state film thickness on the cylindrical heater rod and the average velocity are computed. The steady-state film flow rate is determined in terms of the density, film thickness, and film velocity.

1. Introduction

The in-vessel evolution of a severe accident in a nuclear reactor is characterized by core uncovery, heatup, core material oxidation, heatup acceleration and melting, molten pool formation in the core region, molten material relocation and debris behavior in the lower plenum up to vessel failure [1,2]. The core melt progression [3,4] is characterized by two different phases. One is the early phase referring to the damage occurring between the initial fuel and control rod damage and the melting and relocation of metallic materials. The other is the late phase corresponding to the melting of ceramic material, loss of core geometry, and molten material relocation to the lower plenum of reactor vessel.

Quite a few experimental and analytical efforts were poured to investigate the core melt progression [5]. Results from the separate- and integral-effect core melt progression experiments and from the examination of the damaged core of the Three Mile Island Unit 2 (TMI-2) reactor comprise an important source of data. A status report on the degraded core issues [6] indicates that the early phase of core melt progression is reasonably well understood. Remaining uncertainties may be addressed on the basis of ongoing experimental activities, e.g. on core quenching. Although the experiment using the simulant material instead of the prototypic material tends to have a limit, this will certainly help understand the relevant core melt progression phenomena and contribute to material and geometrical scaling.

The simulant fuel rod was fabricated as shown in Fig. 1. The rod consists of a stainless steel heater, 80cm long and 1cm in diameter, and the simulant material cladding, 2.25mm thick. The simulant material used as the cladding for the experiments was a low-temperature melting metal alloy with a composition by weight percentages of 49.92% Bi, 26.93% Pb, 13.28% Sn, and 9.85% Cd, and the melting temperature of 70℃. This alloy had a density of 9383.2 kg/m^3, a specific heat of 167.5 J/kg·K, a coefficient of volumetric expansion of 2.2×10^{-5} /K, a thermal conductivity of 18.8 W/m·K, and a kinematic viscosity of 2×10^{-7} m^2/s.

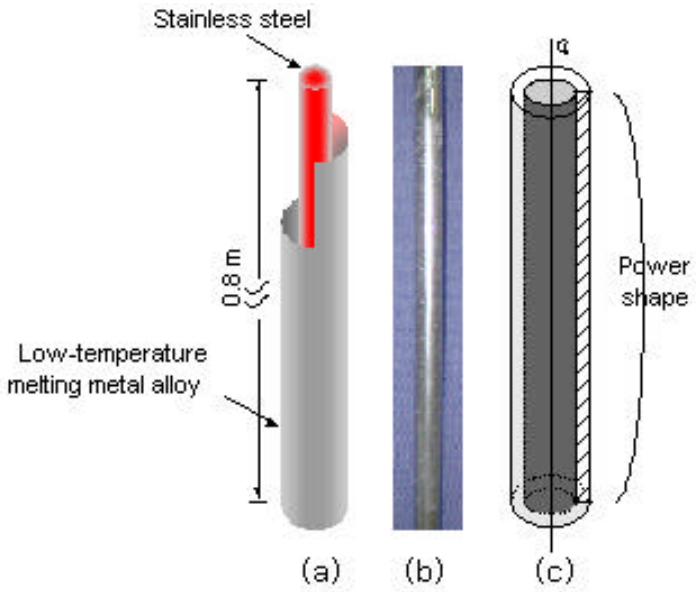

Fig. 1. Experimental Heater Rod

2. Methodology

2.1. Numerical formulation using the ADI (Alternating direction Implicit) method

The following assumptions were made for the physical model and the basic equations.

- Thermophysical properties of the material undergoing phase change are independent of temperature and are evaluated at the film temperature.
- The density variation in the liquid is neglected since the natural convection is not considered in the melt region, which relates to the buoyancy force.
- Volume change due to solid-liquid phase change is negligible.
- Liquid is assumed to be Newtonian.

Consider the two-dimensional heat equation as shown in Fig. 2. Under the transient conditions with constant properties and no internal generation, the appropriate form of the heat equation is

$$\frac{1}{\alpha}\frac{\partial T}{\partial t} = \frac{\partial^2 T}{\partial x^2} + \frac{\partial^2 T}{\partial y^2} \tag{1}$$

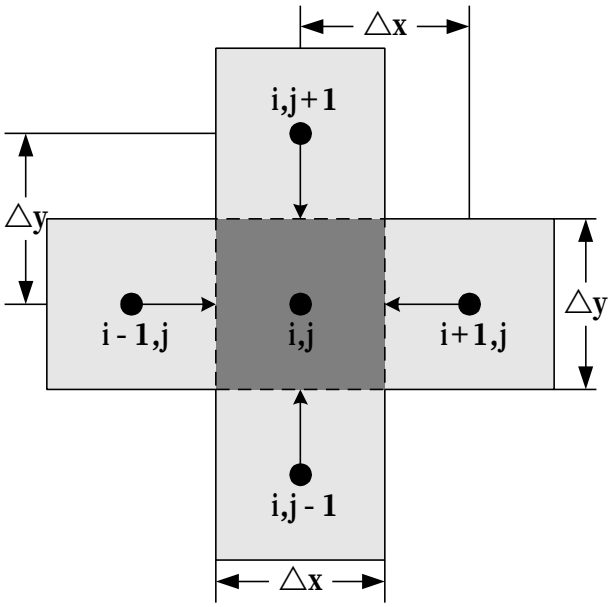

Fig. 2. Conduction to an Interior Node

Ozisik [7] showed that the simple implicit method is used for the x direction and the simple explicit method is used for the y direction to advance from the (n)th to the (n+1)th time level, whence the finite difference approximation to Eq. (1) is given by

$$\frac{T_{i,j}^{n+1} - T_{i,j}^{n}}{\alpha \Delta t} = \frac{T_{i-1,j}^{n+1} - 2T_{i,j}^{n+1} + T_{i+1,j}^{n+1}}{(\Delta x)^2} + \frac{T_{i,j-1}^{n} - 2T_{i,j}^{n} + T_{i,j+1}^{n}}{(\Delta y)^2} \tag{2}$$

For the next time level, that is advance from the (n+1)th to the (n+2)th time level, the simple explicit method is used for the x direction and the simple implicit method is used for the y direction.

$$\frac{T_{i,j}^{n+2} - T_{i,j}^{n+1}}{\alpha \Delta t} = \frac{T_{i-1,j}^{n+1} - 2T_{i,j}^{n+1} + T_{i+1,j}^{n+1}}{(\Delta x)^2} + \frac{T_{i,j-1}^{n+2} - 2T_{i,j}^{n+2} + T_{i,j+1}^{n+2}}{(\Delta y)^2} \tag{3}$$

For computational purposes, it is convenient to rearrange Eqs. (2) and (3) at each time level so that the unknown temperatures appear on the left side and the known temperatures appear on the right side. Thus Eqs. (2) and (3), respectively, become

$$-r_x T_{i-1,j}^{n+1} + (1 + 2r_x) T_{i,j}^{n+1} - r_x T_{i+1,j}^{n+1} = r_y T_{i,j-1}^{n} + (1 - 2r_y) T_{i,j}^{n} + r_y T_{i,j+1}^{n} \tag{4}$$

for the time level n+1, and

$$-r_y T_{i,j-1}^{n+2} + (1 + 2r_y) T_{i,j}^{n+2} - r_y T_{i,j+1}^{n+2} = r_x T_{i-1,j}^{n+1} + (1 - 2r_x) T_{i,j}^{n+1} + r_x T_{i+1,j}^{n+1} \tag{5}$$

for the time level n+2, where $r_x = \frac{\alpha \Delta t}{(\Delta x)^2}$ and $r_y = \frac{\alpha \Delta t}{(\Delta y)^2}$.

Fig. 3 represents the shaded area of Fig. 1-(c). The azimuthal temperature distribution is ignored so that only the radial and axial temperature distributions are accounted for. Fig. 3 shows that rows of 1 and 81 and column of 6 are concerned with natural convection heat transfer. Hence one can obtain the finite difference approximation using the constant temperature boundary condition. Column 1 is a point of contact of the heater and the cladding where heat is supplied. Instead of the constant wall temperature we consider the heater power shape as a cosine shape. The heatup rate is about 0.8K/s and the heater power is monitored by a controller after 130sec to avoid excessive heating, which may cause cladding damage. From the initial and boundary conditions one can obtain a tridiagonal matrix and finally the numerical solutions, i.e. the temperature distribution can be found by the simple matrix inversion method.

2.2. Enthalpy method

The problem of solid-liquid phase change belongs to the class of the so-called “moving boundary problem” due to the existence of the moving phase changing boundary. The mathematical formulation of the phase change problems consists of the transient heat conduction equations for the solid and liquid phases and the interface energy balance equation subject to appropriate boundary and initial conditions.

In the enthalpy formulation, the enthalpy function H(T), which is the total heat content of the substance, enters the problem as a dependent variable along with the temperature. The enthalpy formulation of the phase change problem is given by

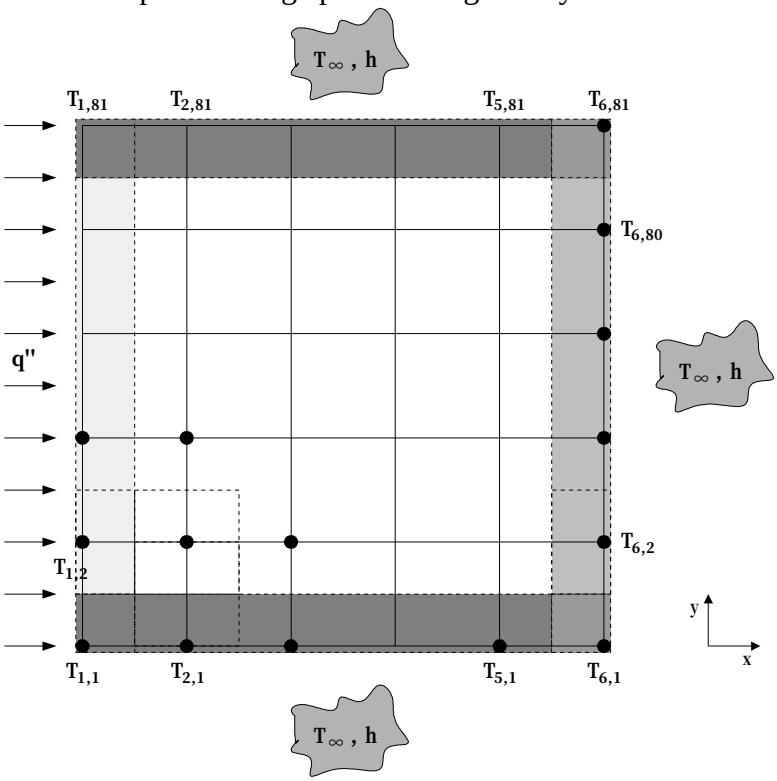

Fig. 3. Two-Dimensional Node Configuration

$$\rho \frac{\partial H(T)}{\partial t} = \nabla \cdot (k \nabla T) \tag{6}$$

Eq. (6) is considered valid over the entire solution domain, including both the solid and liquid phases as well as the solid-liquid interface. There is no internal energy generation. The enthalpy of the material, which is the total heat content, can be expressed as

$$H = h + \Delta H \tag{7}$$

i.e. the sum of the sensible heat, h=CpT, and the latent heat ? H. When some node temperature reaches the melting point the temperature will no longer increase until the node enthalpy exceeds the latent heat of fusion. Fig. 4 shows the enthalpy-temperature relation. In numerical analysis of the simulant material the phase change takes place at a discrete temperature associated with the latent heat and a discontinuity occurs at the melt temperature T_m. The solid-liquid interface grows and defines the boundary condition, which divides the solid phase heat conduction region from the liquid phase heat conduction region.

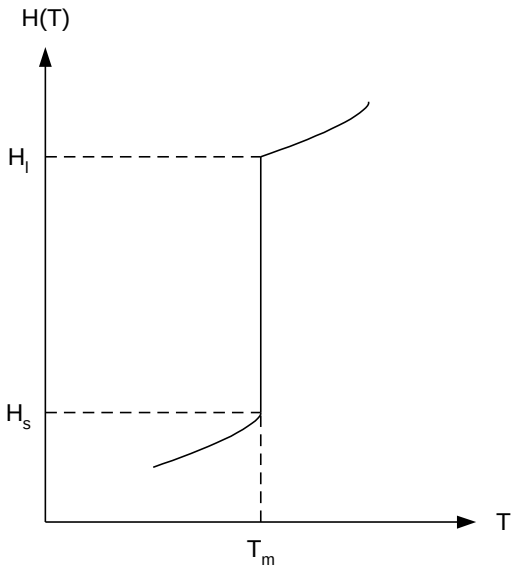

Fig. 4. Enthalpy-Temperature Relation

3. Results

Widespread melting can occur once the temperature reaches the cladding melting point of about 2200K in case of the prototype material. Some models were developed to describe the dripping of the liquefied fuel and cladding down the outside of fuel rods such as film flow or pipe flow and to calculate where the material solidifies and blockage forms. The prototype fuel rod is composed of high melting point materials such as UO_2, ZrO_2 and Zr, which undergo rather complex thermochemical reactions. Instead, we used a low-temperature melting material to simulate the melt progression on the laboratory scale. Because of the material properties, however, the heat flux was quite limiting. Although the loss-of-coolant accident (LOCA) is a transient condition, current experiments and analysis were conducted in several quasi-steady-state conditions. Numerical analysis for the node temperature prediction was conducted until the cladding integrity was maintained so that there was no cladding surface melting.

Fig. 5 illustrates the temperature distribution in the totally uncovered cladding. In this case there is no heat removal by the coolant and the axial power takes on a chopped cosine shape such that the melt progression is initiated at the mid-point. Because the height-to-thickness ratio y/x=356 is so large with the thickness being merely 2.25mm, the surface temperature reaches the melting point early and the melt region quickly spreads axially. In the experiments one could observe incipience of molten liquid bubbles of 1 to 2mm in diameter on the fuel rod surface.

Fig. 6 shows the temperature distribution in the rod partially covered with water 20cm from the bottom of the heater rod. In this case there is no melt formation below the water level. Above the water level rather mild temperature gradient is generated. Additionally the melt region is less spread axially relative to the case of totally uncovered rod. Fig. 7 shows the temperature distribution in the rod covered with water 40cm from the bottom. Again, there is no melt formation below the water level. Above the water level, rather gradual

temperature gradients are generated, as was the case with the rod partially covered up to 20cm. The melt region is much less spread axially relative to the previous two cases.

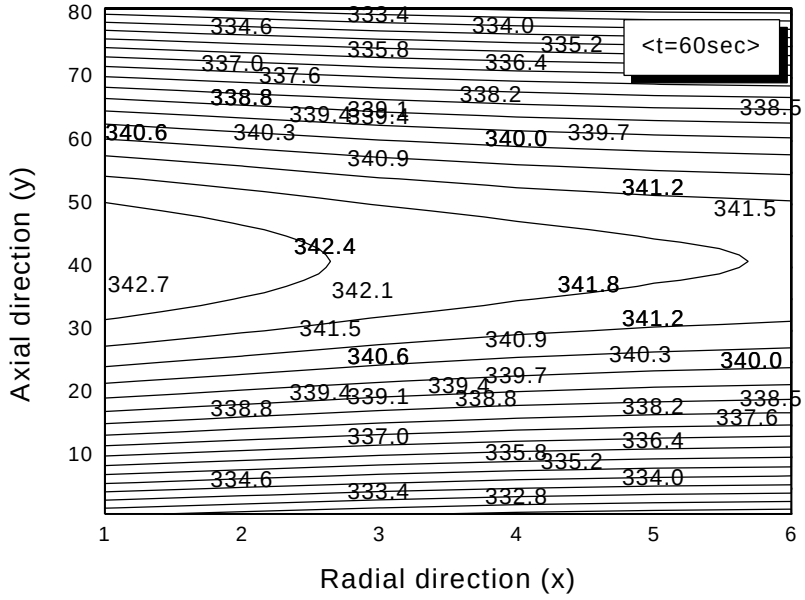

Fig. 5. Temperature Distribution at 60sec (Uncovered)

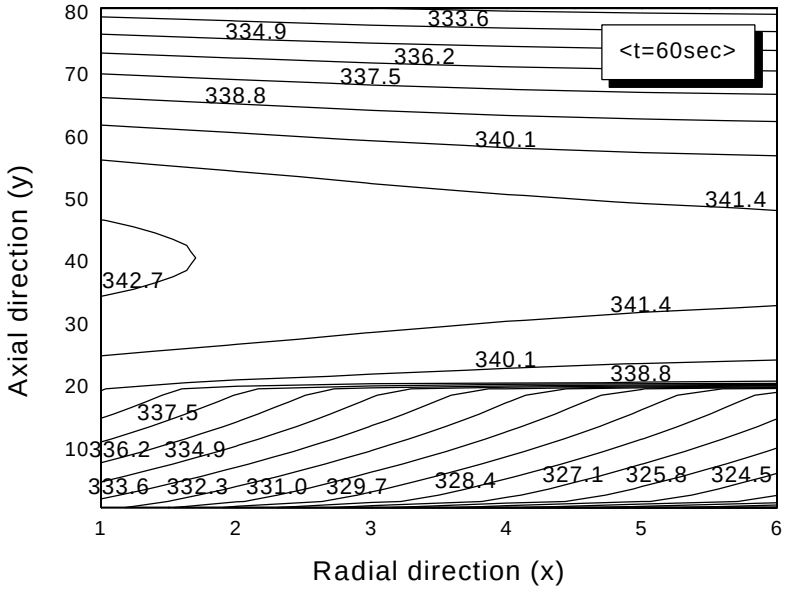

Fig. 6. Temperature Distribution at 60sec (20cm Covered)

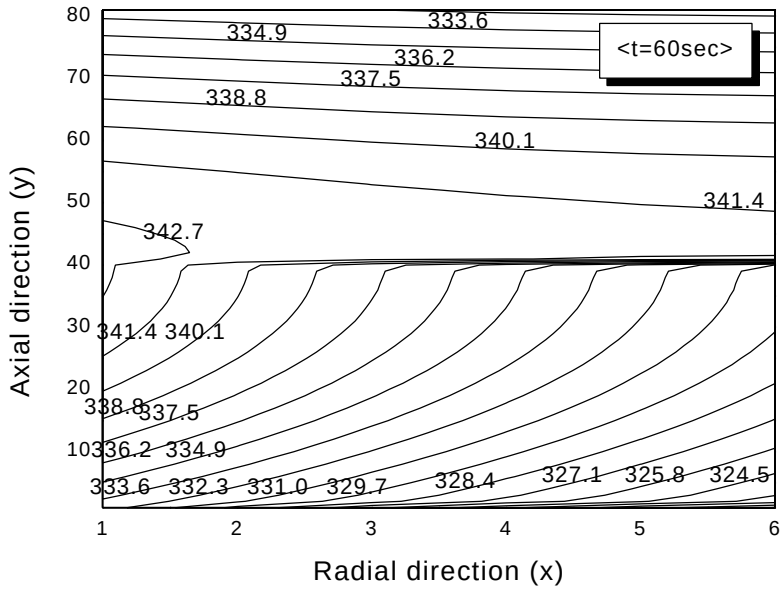

Fig. 7. Temperature Distribution at 60sec (40cm Covered)

Fig. 8 shows the solid-liquid interface during melting in the totally uncovered case. The melting begins at the point of heater and cladding contact surface but the melt region is narrow early in the test. As time progresses the melt region grows.

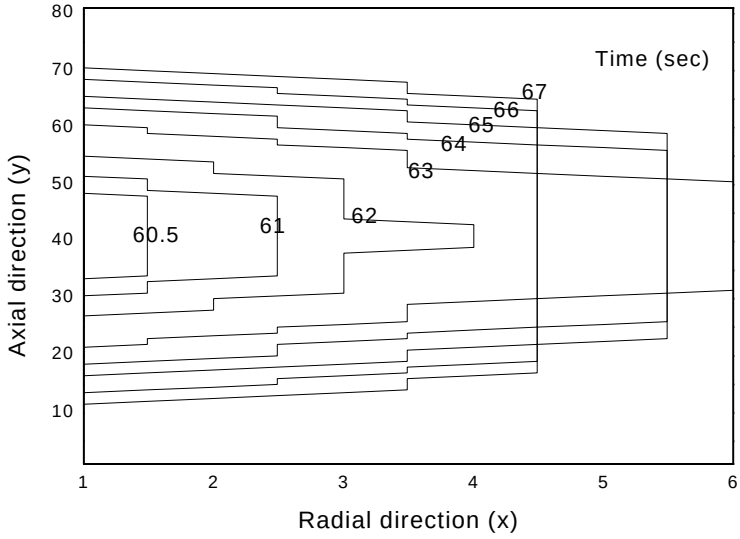

Fig. 8. Interface Contour at Selected Times during Melting

Analytical solutions of the phase change problems are known only for a handful of physical situations with simple geometries and boundary conditions such as the Neumann problem [8-13]. A number of analytical and experimental studies were performed for the mathematical modeling and the experimental measurements of the moving boundary problems.

Starting from the basic knowledge on the pre-melting phase, i.e. as much as the cladding integrity is maintained, one can construct a fuel melt progression model for the post-melting as shown in Fig. 9.

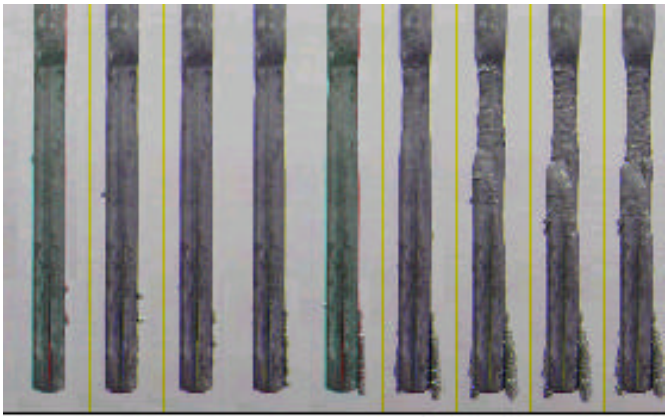

Fig. 9. Melt Progression Simulation

Fig. 10 shows the temperature distribution inside the cladding when the outer surface temperature reaches the melting point for the water level at 10cm. Fig. 11 to Fig. 17 each shows the temperature distribution inside the cladding at different water levels. When the water covers the fuel rod over 75cm no melt progression is predicted. The melt region is less spread axially. The melt location rises with the water level. In case of the cosine power shape, when the water level is below the center of the fuel rod there is calculated to be no effect on the initial surface melting time except that the melting is delayed as the water level increases. Fig. 18 finally shows the melting time and location for differing water temperatures.

4. Conclusion

In this paper we focused mostly on the simple and parametric numerical analysis, while the experiments are still in progress. The enthalpy method is a simple model for solving the moving boundary problems associated with melting. We did not consider the natural convection induced by the temperature difference in the liquid melt. In the simple approach the quantity of melt relocation is dependent on the numerical representation of the geometry or the finite difference nodalization. The accuracy in the melt progression model will be improved by temperature comparison between predictions and experiments. The coolant level and temperature affects melt location and time so these are dominant parameter in the melt progression simulation test. Additionally we consider different power shape. The current model can be extended to the natural convection heat transfer in the molten pool.

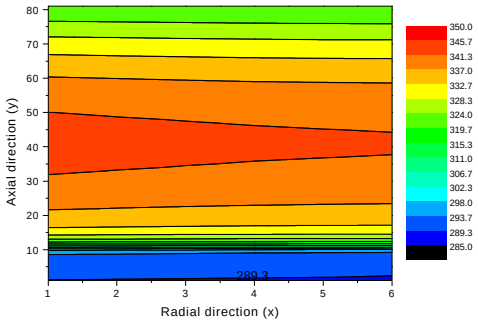

Fig. 10. Temperature Profile at Water Level = 10cm

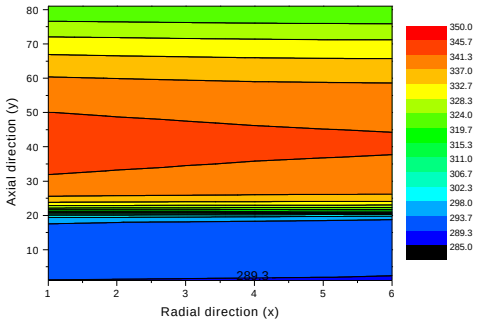

Fig. 11. Temperature Profile at Water Level = 20cm

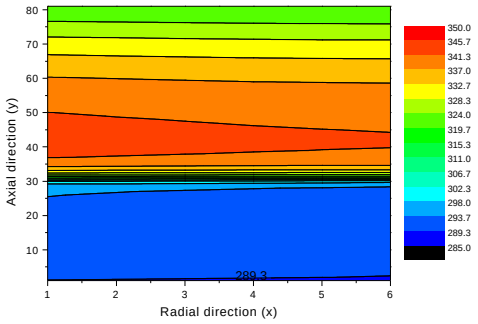

Fig. 12. Temperature Profile at Water Level = 30cm

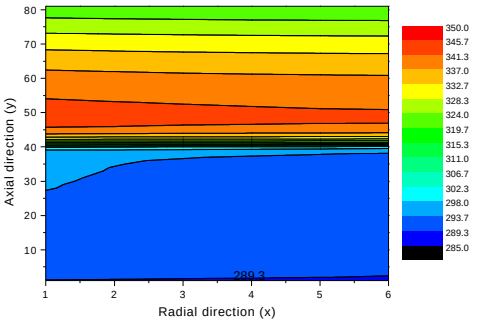

Fig. 13. Temperature Profile at Water Level = 40cm

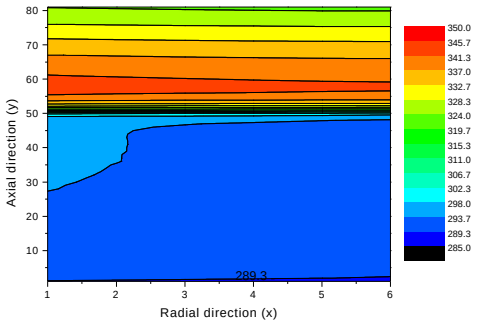

Fig. 14. Temperature Profile at Water Level = 50cm

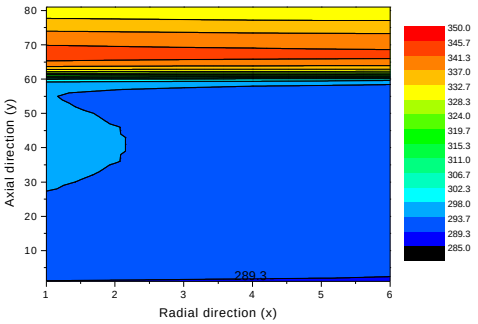

Fig. 15. Temperature Profile at Water Level = 60cm

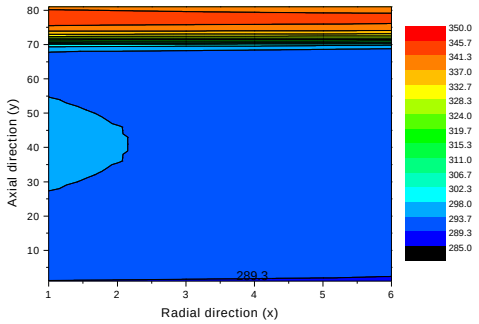

Fig. 16. Temperature Profile at Water Level = 70cm

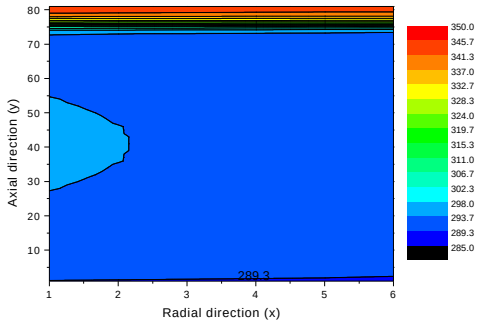

Fig. 17. Temperature Profile at Water Level = 75cm

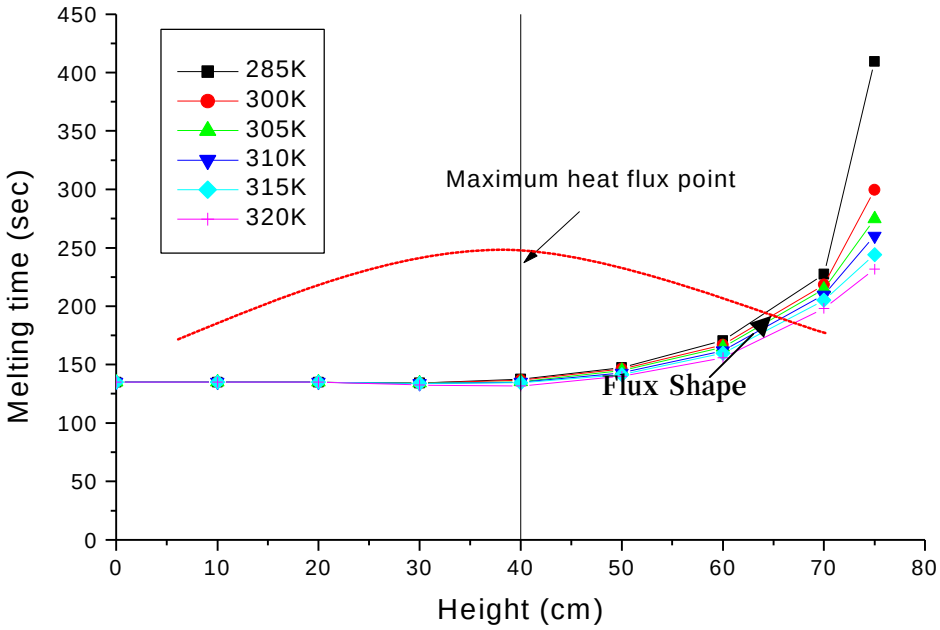

Fig. 18. Melt Progression at Differing Water Temperatures

Nomenclature

Cp	specific heat
? x	radial mesh size
? y	axial mesh size
H	enthalpy
H_s	solid enthalpy
H_l	liquid enthalpy
h	sensible heat
L	latent heat of melting
T	temperature
T_m	melting temperature
? t	time step

Greek symbols

a	thermal diffusivity
ß	volumetric expansion coefficient

Superscript		Subscripts	
n	time level	i	column node
		j	row

References

1. Hobbins R.R., Petti D.A., Osetek D.J., “Review of experimental results on light water reactor core melt progression,” Nuclear Technology, Vol. 95, (1991) 287-307
2. Hofmann P., “Current knowledge on core degradation phenomena, a review,” Journal of Nuclear Materials, 270, (1999) 194-211
3. Haste T.J. et al., “In-Vessel Core Degradation in LWR Severe Accident: A State of the Art Report,” EUR 16695 EN, European Commission, (1996a)
4. Haste T.J. et al., “In-Vessel Core Degradation. Code Validation Matrix,” OECD/GD(96)14, NEA/CSNI/R(95)21, (1996b)
5. Lillington J.N., “Light water reactor safety: the development of advanced models and codes for light water reactor safety analysis,” Elsevier Science, B.V., Amsterdam, The Netherlands (1995)
6. G. Bandini. et al., “Status of Degraded Core Issues,” OECD NEA/CSNI/R(2001)5, October, (2000)
7. Ozisik M.N., “Finite difference methods in heat transfer,” (1994)
8. Hongfa H., Stavros A.A., “Mathematical modeling and experimental measurements of moving boundary problems associated with exothermic heat of mixing,” International Journal of Heat and Mass transfer, Vol. 39, No. 5, (1996) 1005-1021
9. Shastri S.S., Allen R.M., “Method of lines and enthalpy method for solving moving boundary problems,” International Communication Heat Mass Transfer, Vol. 25, No. 4, (1998) 531-540
10. Gau C., Viskanta R., “Melting and solidification of a pure metal on a vertical wall,” Journal of Heat Transfer, Transactions of the ASME, Vol. 108 (1986)
11. Cho S.H., “Phase change problems with temperature-dependent thermal conductivity,” Journal of Heat Transfer, Transactions of the ASME, (1974) 214-217
12. Ho C.J., Viskanta R., “Heat transfer during melting from an isothermal vertical wall,” Journal of Heat Transfer, transactions of the ASME, Vol. 106 (1984) 12-19
13. Sparrow E.M., Patankar S.V., Ramadhyani S., “Analysis of melting in the presence of natural convection in the melt region,” Journal of Heat Transfer, Transactions of the ASME, Vol. 99, (1974) 520-526